Monte Carlo simulation of a single-molecule detection experiment

Dennis H. Bunfield and Lloyd M. Davis

The physical and instrumental processes that occur in experiments for the detection of individual fluorescent molecules in solution are described, with emphasis on their incorporation into a quantitative Monte Carlo simulation. The simulation is applied to the conditions of a past experiment [Appl. Opt. **34,** 3208 (1995)], which utilizes a sheath flow system for high detection efficiency, and it generates comparable results, while helping to identify experimental limitations. The simulation indicates that the use of low dead-time electronics and appropriate selection of experimental parameters should enable detection at more rapid rates for applications in which large numbers of molecules are to be efficiently counted.

OCIS codes: 120.0120, 170.6280, 300.2530, 040.1880.

1. Introduction

Single-molecule detection (SMD) in solution has many applications in biotechnology and analytical chemistry currently under development.[1] A quantitative understanding of the factors that contribute to the detection process is important for advancing the state of the art. Since the first report of the detection of individual single-chromophore molecules in bulk aqueous solution,[2] there have been several improvements in experimental capabilities, which have resulted in SMD becoming more widely available. Aside from the recent achievement of SMD with use of surface-enhanced Raman scattering[3,4] rather than fluorescence photon-burst detection, the advancements have for the most part been due to two items: (1) the use of high-quantum-efficiency single-photon avalanche diode (SPAD) detectors to give higher fluorescence sensitivity[5] and response in the near infrared[6,7] and/or (2) the use of subfemtoliter probe volumes obtained by epiillumination and confocal imaging with a high-numerical-aperture (NA) objective,[8,9] or by a thin-layer of solution,[10] to yield less background from solvent and impurity molecules and sufficient intensities for two-photon excitation of fluorescence.[11]

Several of the reported experimental advances in SMD have mentioned the use of Monte Carlo simulations to gain confidence in the interpretation of results[2,12,13] and to help in the selection of appropriate experimental parameters.[14] However, the details of which physical processes are important and how they can be simulated have not been explained in the literature.

For the design of SMD experiments in solution, there are many factors that influence the levels of signal and background noise, and compromises must be made in the selection of operating parameters.[15,16] If the application requires identification of individual molecules by performing spectroscopic measurements,[17,18] then the signal level from each molecule, which influences the measurement precision, will be important. The application of the simulation to this situation is discussed elsewhere.[19,20] In this paper we discuss applications in which the goal is to rapidly and efficiently detect all molecules within a small sample.[1] In this case, the signal level from each detected molecule is not of paramount importance, provided it is greater than the fluctuations in the background. The equations and methods discussed here are for the most part general, and the simulation can be applied to other applications with little modification.

In section 2 we explain the choice of the experimental setup of Ref. 1 that is used to achieve high overall molecule detection efficiency, and we give an overview of the physical processes that can occur during detection that must be included in the simulation. In Section 3 we then detail each of the physical pro-

The authors are with the Center for Laser Applications, University of Tennessee Space Institute, Tullahoma, Tennessee 37388.

Received 17 July 1997; revised manuscript received 18 December 1997.

0003-6935/98/122315-12$15.00/0

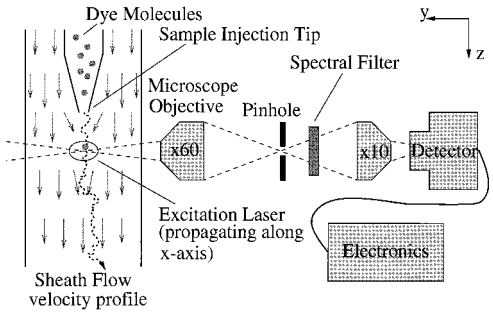

Fig. 1. Schematic of flow cell and experimental setup. A beam of picosecond pulses from a synchronously pumped dye laser is focused into an 800-μm square-bore capillary. Fluorescence from molecules transiting the beam is collected at right angles, spatially filtered, spectrally filtered by an interference filter, and focused onto a SPAD. Raman scatter from the solvent that overlaps the fluorescence band is discriminated with use of a custom-built subnanosecond time-gating circuit and also a time-to-amplitude converter, fast digitizer, and software filter. The digitized data stream is further filtered to identify individual molecule transits. See Ref. 1 for further details.

cesses and explain how each is simulated. In Section 4 we present results from the simulation under the conditions of Ref. 1 and of an experiment under development, which uses an actively quenched SPAD detector with low dead time[21] in an attempt to achieve higher molecule detection rates. In Section 5 we conclude with a overview of other applications of the simulation.

2. Setup for Efficient Detection

In most prior experiments, only a small fraction of the analyte molecules pass through the probe region, and consequently the overall detection efficiency is low. Usually a sample cell with dimensions considerably larger than that of the probe region is used so that scattered light and induced fluorescence from the cell walls can be rejected effectively by a spatial filter. Also, if diffusion dominates the transport of molecules, as in experiments that utilize subfemtoliter-sized probe regions, there is a nonnegligible probability that subsequent photon bursts will be due to the same molecule reentering the probe region.[22] To efficiently detect and count all molecules within a sample without overcounting,[23] the probe region must be sufficiently large and the flow rate sufficiently fast that transport is dominated by the bulk flow, and also the molecules must be confined in some manner so that all will pass through the probe region. However, the flow rate must also be sufficiently slow that molecules spend an adequate time transiting the probe region if each is to be detected.

Because of these considerations, to achieve efficient SMD as in Ref. 1, molecules are introduced into a sheath flow through the submicrometer opening of an injection capillary, which is placed immediately upstream from the focused laser beam, as shown in Fig. 1. As molecules are carried by the sheath flow from the tip of the injection capillary to the probe region, they will undergo diffusion, as discussed in Subsection 3.A. Nevertheless, all molecules will pass through the probe region provided that the sheath flow is sufficiently fast and the cross-sectional area of the probe region is sufficiently large.

As each molecule passes through the focused beam, it experiences a laser intensity dependent on its position, leading to various possible interactions, which are discussed in Subsection 3.B. In particular, the molecule may become excited and emit a fluorescence photon as it relaxes to the ground state, and this may happen many times as the molecule transits the beam, thereby resulting in the emission of a burst of photons. The region from which photons are efficiently collected is determined by the microscope objective and pinhole, as discussed in Subsection 3.C, and the overlap of this region with the focused laser beam defines the probe region.

Even when a molecule is not present within the probe region, there is a finite chance that photons may be detected because of background. The various sources of background and their dependence on experimental parameters, such as the probe volume, light collection efficiency, and detector count rate, are discussed in Subsection 3.D. The use of a moderately sized probe region results in high levels of scattered light. Rayleigh-scattered light and most of the Raman-scattered light from solvent molecules is blocked by a spectral filter, but that which overlaps the molecular fluorescence band is passed to the detector. Pulsed excitation from a mode-locked laser and time-gated photon detection can be used to discriminate this promptly scattered Raman light from the nanosecond-delayed fluorescence.[2] However, if a time-to-amplitude converter (TAC) is used in the time-gating electronics, it will introduce a dead time, during which subsequently detected photons are missed. Even without time gating and with cw laser excitation, the SPAD photon detector itself has a dead time that must be accounted for. The simulation of these dead times is discussed in Subsection 3.E, together with a flow diagram of the overall simulation. Methods for processing the data from the stream of detected photons are discussed in Subsection 3.F.

3. Simulation

A. Molecule Transport

The sheath flow is laminar and is approximated to have a constant velocity v, and hence with each iteration, each molecule present is advanced along the z direction by a distance

$$\Delta z = v\Delta t. \tag{1}$$

Here Δt is the duration represented by each iteration, and ideally it should be set to the minimum possible time between successive molecular interactions, which for pulsed excitation is the reciprocal of the laser repetition rate R. To simulate the experiment of Ref. 1, the flow velocity v is set equal to the radius of the laser waist ω_{z0}, divided by the mean molecular

half-transit time δ_t, which is obtained from the experimental autocorrelation function, as explained in Subsection 3.F.

With each iteration a counter, t_1, is incremented. To simulate the injection of molecules at random times, a second counter, t_2, is used to count down the number of remaining iterations until the next molecule injection. When $t_2 = 0$, another molecule is generated at the location $(r \cos \phi, r \sin \phi, -z_0)$, where $r = r_0\sqrt{R_U}$, $\phi = 2\pi R_U$, r_0 is the injection tip's radius, z_0 is its distance from the center of the focused laser waist, and R_U is a uniform random number between 0 and 1. At this time t_2 is assigned a new random number with an exponential deviate and a decay constant equal to the mean time between molecules δt:

$$t_2 = R_{\mathrm{EX}}\delta t, \tag{2}$$

where

$$\delta t = (\pi r_0{}^2[M]N_A\Delta z)^{-1}, \tag{3}$$

$[M]$ is the molar concentration of dye molecules in the sample, and N_A is Avogadro's number. An exponential deviate is used because, for randomly occurring events, the time between successive events is random with an exponential probability density. For high concentrations, t_2 can sometimes be assigned the number 0, in which case more than one molecule would be generated during the present iteration. A simple flow system without an injection capillary can be simulated by setting the parameter r_0 to a value larger than the cross-sectional dimensions of the probe region.

To simulate the diffusional component of the transport of molecules, note that the solution of the diffusion equation $\partial c/\partial t = D\nabla^2 c$ with the initial condition $c(t = 0) = \delta(x, y, z)$ corresponding to a single molecule located at the origin at time $t = 0$, is

$$c = (4\pi Dt)^{-3/2} \exp[-(x^2 + y^2 + z^2)/4Dt]. \tag{4}$$

Here D is the diffusion coefficient, and $c(x, y, z, t)\mathrm{d}x\mathrm{d}y\mathrm{d}z$ represents the probability density for finding the molecule within $\mathrm{d}x\mathrm{d}y\mathrm{d}z$ at the location x, y, z at time t. Therefore, with each iteration, each of the three Cartesian coordinates of the molecule is incremented by an amount $R_G \times 2\sqrt{D\Delta t}$, where R_G is a random number with Gaussian distribution and unity variance.

In addition to translational diffusion, the molecule also undergoes Brownian rotational diffusion, which changes the direction of the absorption transition dipole vector θ, ϕ and hence the square of its component along the laser polarization direction, ζ. If the laser is linearly polarized and the direction of polarization is chosen as the polar axis for measurement of θ, ϕ, then $\zeta = \cos^2 \theta$. If the laser is circularly polarized, then ζ oscillates at optical frequencies and the cycle-averaged value of $\zeta = 0.50$ applies. For single-chromophore molecules in aqueous solution, randomization of orientation, which is due to rotational diffusion, occurs on a time scale of $\tau_r \sim 100$ ps, which is considerably faster than the typical fluorescence lifetime of $\tau_f \sim 3$ ns. In this case, the simulation does not need to follow the molecular orientation, but with each iteration a new value of $\cos^2(\pi R_U)$ is used for ζ. If the chromophore is bound rigidly to a spherically symmetric macromolecule or if a viscous solvent such as glycerol is used, then the angle θ must be recorded between iterations and incremented by $R_G\ 2\sqrt{D_r\Delta t}$ each iteration, where $D_r = \tau_r{}^{-1}$ is the rotational diffusion coefficient.

B. Laser–Molecule Interactions

1. Laser Intensity

As a molecule is transported through the laser beam, the probability that it will become excited per unit time depends on the intensity at its present location, x, y, z, which in turn depends on the focusing of the beam. To increase the cross-sectional area of the probe region in the direction of flow, while maintaining a small probe volume, cylindrical lenses can be used to obtain an elliptical beam with different waists in the y and z dimensions. In general, the waists can occur at different points, x_y and x_z, along the direction of propagation, here assumed to be the x axis. Also, aberrations, caused mainly by focusing of the beam through the walls of the sample cell, can cause the actual beam waists to be a factor M_y or M_z times larger than that of the ideal diffraction-limited Gaussian beam, i.e.,

$$\bar{\omega}_{i0} = M_i\omega_{i0}, \quad i = y, z. \tag{5}$$

Under these general conditions, for a laser power P, the peak intensity is

$$\hat{I} = 2P/(\pi\bar{\omega}_{y0}\bar{\omega}_{z0}), \tag{6}$$

and the intensity at x, y, z relative to $\hat{I}$ is

$$I(x, y, z) = \prod_{i=y,z} \frac{\bar{\omega}_{i0}}{\bar{\omega}_i(x)} \exp\left[\frac{-2i^2}{\bar{\omega}_i{}^2(x)}\right], \tag{7}$$

where the beam sizes are

$$\bar{\omega}_i{}^2(x) = \bar{\omega}_{i0}{}^2\{1 + [(x - x_i)/x_{i0}]^2\}, \tag{8}$$

the Rayleigh ranges are

$$\bar{x}_{i0} = \pi\bar{\omega}_{i0}{}^2/(M_i{}^2\lambda) = x_{i0}, \tag{9}$$

and $\lambda = \lambda_0/n$, where λ_0 is the wavelength of the laser in air and n is the refractive index of the solution.

2. Molecular Excitation

The probability of molecular excitation also depends on the characteristics of the laser beam. If the laser has a bandwidth that is narrow compared to that of the dye molecule's absorption spectrum, it will couple the ground state to only a small subset of vibrational sublevels of the electronic excited state. The excited-state wave function dephases on the time scale of the collisions with solvent molecules, so that unless laser pulses of comparable duration <100 fs are used, the optical Bloch equations can be replaced by simpler rate equations.[24] The rate for absorption

from the ground state K is then proportional to the absorption cross section σ_a; the transition dipole orientation factor ζ that was introduced in Subsection 3.A; and the photon flux, i.e.,

$$K = \sigma_a \zeta \hat{I} I(x, y, z)/E_\gamma, \tag{10}$$

where E_γ is the energy of each photon.

If the laser wavelength is shorter than the maximum wavelength of the molecular absorption spectrum, the subset of laser-coupled vibrational sublevels that become depopulated by thermalization of the vibrational manifold is due to collisions with solvent molecules on a time scale of $\tau_v \sim 0.5$–1 ps,[25] which is $\ll \tau_f$. In this case, the molecule can be approximated as a three-level system with rate equations

$$\frac{\mathrm{d}}{\mathrm{d}t}\begin{bmatrix} P_0 \\ P_1 \\ P_2 \end{bmatrix} = \begin{bmatrix} -K & K & \tau_f^{-1} \\ K & -K + \tau_v^{-1} & 0 \\ 0 & \tau_v^{-1} & \tau_f^{-1} \end{bmatrix}\begin{bmatrix} P_0 \\ P_1 \\ P_2 \end{bmatrix}, \tag{11}$$

where P_0, P_1, and P_2 represent the probabilities that the molecule is in the ground level, the vibrationally and electronically excited level, and the ground-vibrational electronic-excited level, respectively. The equations could be solved for the initial condition $P_0 = 1, P_1 = P_2 = 0$, corresponding to the molecule in the ground state to find the dependence of the probability of excitation on the laser power and hence the saturation behavior. However, for pulsed excitation, further approximations can be made.

If the pulse duration is short compared to the fluorescence lifetime, τ_f^{-1} can be set equal to zero in Eq. (11). If the pulses are taken to have a Gaussian profile with full-width at half-maximum, $\tau_p = 2\sqrt{2 \ln 2}\, \sigma_t$, the peak power is

$$\hat{P} = \bar{P}/(\sqrt{2\pi}\, R\sigma_t), \tag{12}$$

where $\bar{P}$ is the average power, and the instantaneous power is

$$P(t) = \hat{P} \exp[-t^2/(2\sigma_t^2)]. \tag{13}$$

The absorption rate changes in time as

$$K(t) = \hat{K} \exp[-t^2/(2\sigma_t^2)], \tag{14}$$

where the peak absorption rate for a molecule located at x, y, z is

$$\hat{K} = 2\sigma_a \zeta(t) \hat{P} I(x, y, z)/(\pi \bar{\omega}_{y0} \bar{\omega}_{z0} E_\gamma). \tag{15}$$

If the pulse duration is faster than the rotational diffusion time, $\tau_p \ll \tau_r$, the orientation factor ζ will be constant during each pulse. Furthermore, if $\hat{K} \ll \tau_v^{-1}$ then stimulated emission back to the ground state during the pulse can be ignored. If the ground state is not appreciably depleted, the probability of excitation to level 2 per laser pulse is

$$P_E = \int K(t)\mathrm{d}t, \tag{16}$$

where

$$\int K(t)\mathrm{d}t = 2\sigma_a \zeta \bar{P} I(x, y, z)/(\pi \bar{\omega}_{y0} \bar{\omega}_{z0} E_\gamma R). \tag{17}$$

Otherwise, saturation occurs, and

$$P_E = 1 - \exp\left[\int K(t)\mathrm{d}t\right]. \tag{18}$$

Note that $P_E \to 1$ can occur if $\tau_p \gg \tau_v$. For the conditions of the experiment of Ref. 1, which uses pulses of duration $\tau_p \sim 10$ ps at a repetition rate of $R = 7.6 \times 10^7\ \mathrm{s}^{-1}$, for a molecule at the origin with $\zeta = 1$, Eqs. (15) and (12) yield a value of $K = \tau_v^{-1} = (1\ \mathrm{ps})^{-1}$ for an average laser power of $\bar{P} = 0.5$ W, and hence, provided that the average laser power is below this value, Eq. (18) is accurate. On the other hand, if $\hat{K} \gg \tau_v^{-1}$, stimulated emission must be considered in determining the form of saturation. In this case, if $\tau_p \ll \tau_v$, as is the case for excitation with subpicosecond laser pulses,[6] saturation is such that the probability of excitation per laser pulse is at most 0.50 with

$$P_E = \left\{1 - \exp\left[\int K(t)\mathrm{d}t\right]\right\}/2. \tag{19}$$

3. Molecular Deexcitation

Once a molecule is excited, it may return to the electronic ground state by some quenching mechanism without the release of a fluorescence photon. This need not be followed in the simulation because it leads to no consequential effects in the experiment.

The molecule may return to the ground state by an electric dipole radiative transition with the release of a fluorescence photon. The probability for such a photon to be emitted per iteration is

$$P_f = P_E \Phi_f \Delta t/R, \tag{20}$$

where Φ_f is the fluorescence quantum efficiency. The time between excitation and emission is random with an exponential distribution with the mean equal to the fluorescence lifetime τ_f. If this is slower than the rotational diffusion time, i.e., if $\tau_f \gg \tau_r$, the fluorescence emission will be isotropic in space and of random linear polarization.

Alternately, the molecule may intersystem cross to the triplet manifold. The probability per iteration that this occurs is

$$P_{\mathrm{isc}} = P_E \Phi_{\mathrm{isc}} \Delta t/R, \tag{21}$$

where Φ_{isc} is the quantum efficiency for intersystem crossing. From here, the molecule may become photodestroyed with a probability per iteration of

$$P_d = P_E \Phi_d \Delta t/R, \tag{22}$$

where Φ_d is the photodestruction quantum efficiency. If the molecule is not to become photodestroyed, it will remain in the triplet manifold until it relaxes to

the ground state, usually by some nonradiative mechanism. In this case, the number of subsequent iterations for which the molecule is unavailable is random with an exponential deviate and a decay constant proportional to the phosphorescence lifetime τ_{ph}, typically $\sim 10^{-6}$ s. In the simulation, a counter associated with the particular mth molecule in question, t_m, is assigned a random number with exponential deviate $t_m = R_{EX}(\tau_{ph}/\Delta t)$. In each iteration, the counter for each molecule is first checked, and if it is nonzero it is decremented so as to count down the remaining number of iterations the molecule will spend in the triplet manifold, and calculations of P_E and subsequent laser interactions are not performed for that molecule.

C. Light Collection and Detection

Two counters t_S and t_T are also used to account for the dead times of the SPAD detector and the TAC of the time-gating electronics. If $t_S = 0$, indicating that the SPAD is responsive, the net probability for detection of a fluorescence photon during the present iteration must be evaluated, and hence for each molecule present that is not in the triplet manifold, the probability of fluorescence P_f and the collection efficiency of light from the present location of the molecule must be calculated.

If the fluorescence emission is isotropic, the maximum efficiency with which light is collected $\hat{C}$ is determined by the fraction of the solid angle subtended by the NA of the microscope collection objective:

$$\hat{C} = (1 - \cos\alpha)/2, \tag{23}$$

where

$$\alpha = \sin^{-1}(\mathrm{NA}/n), \tag{24}$$

and n is the refractive index of the solution. The maximum collection efficiency is obtained if the molecule is at the origin, i.e., at the center of the object space virtual image of the spatial filter. If the molecule is located elsewhere when it emits the photon, the collection efficiency may be reduced.

The collection efficiency from a molecule located at x, y, z relative to the maximum value $C(x, y, z)$ can be evaluated by calculation of the overlap of the out of focus image of the emission point with the aperture of the spatial filter, as shown in Fig. 2. If aberrations in the collection optics are negligible and if the NA of the microscope objective is moderate ($\leq$0.85) so that the point spread function of the collection optics is finite in a region much smaller than the spatial filter aperture, then geometric ray tracing provides an adequate calculation of the out of focus image. In this case, for a circular pinhole spatial filter, $C(x, y, z)$ is obtained in terms of a two-dimensional convolution integral of two circular disk functions [see Eq. (3) in Ref. 24]. To evaluate the convolution, note that as illustrated in Fig. 2, the overlap area A between two disks of radii 1 and Z with centers separated by a distance R can be found as the sum of the two circular segments subtended by angles β and γ:

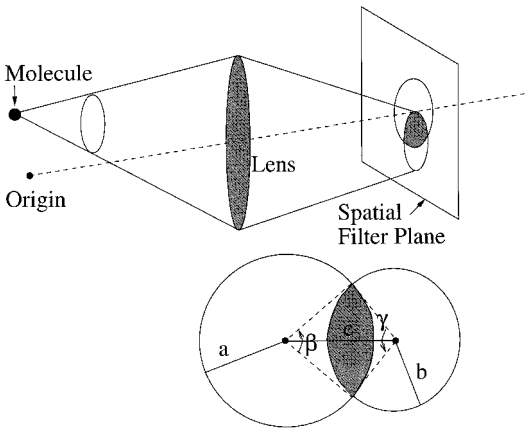

Fig. 2. Determination of the efficiency of light collection through the spatial filter.

$$A(1, Z, R) = \beta + \gamma Z^2 - (\sin 2\beta + Z \sin 2\gamma)/2, \tag{25}$$

where

$$\beta = \cos^{-1}[(1 + R^2 - Z^2)/2R], \tag{26}$$

$$\gamma = \cos^{-1}[(Z + R^2 - 1^2)/2RZ]. \tag{27}$$

Using these results in Eq. (3) of Ref. 24 we obtain

$$C(R, Z) = \begin{cases} 1, & 0 < Z < 1 - R \\ A(1, Z, R)/(\pi Z^2), & 1 - R < Z < 1 + R \\ [1 - (Z/\sqrt{\tan^2\alpha + Z^2})]/(2\pi\hat{C}) & \\ & 1 + R < Z < R - 1 \\ 0, & R - 1 < Z \end{cases}, \tag{28}$$

where Z is the normalized coordinate along the axis of the collection objective, defined by

$$R = y \tan\alpha/s_0, \tag{29}$$

R is the normalized radial coordinate, defined by

$$R = \sqrt{x^2 + z^2}/s_0, \tag{30}$$

and s_0 is the radius of the virtual image of the spatial filter, which is the pinhole radius r_p divided by the magnification of the objective M. If aberrations or diffraction effects are significant, then a better approximation for $C(x, y, z)$ can be obtained by convolution of Eq. (28) with the three-dimensional point spread function of the optics. This results in a smoothing of the function $C(x, y, z)$, but the difference is reportedly small if a high-quality, moderate NA microscope objective is used.[26]

D. Sources of Background

When time-gated photon detection is used to discriminate promptly scattered light, background photons that are rejected by the time gate must still be accounted for as they may lead to significant dead time

of the SPAD detector. The actual levels of background counts that are passed and rejected by the time gate, $\bar{b}$ and $\bar{b}'$, can be measured with pure solvent under well-characterized experimental conditions and then used to obtain the values of empirical constants β and β', which in turn are used by the simulation to predict the background levels b and b' under different experimental conditions. To do this, a model of the dependence of the various sources of background on experimental parameters such as laser power, beam waist sizes, diameter of spatial filter, etc., is needed. To this end, the major sources of background are as noted below.

1. Detector Dark Noise

This is due largely to the thermal generation of avalanche pulses in the SPAD detector. The rate of dark counts that are passed by the time gate b_D will be independent of experimental parameters and can be measured by blocking the laser beam. Dark counts blocked by the time gate make a negligible effect on the SPAD dead time.

2. Promptly Scattered Photons

These will be due mostly to Raman scatter from solvent molecules, as the spectral filter should block Rayleigh scatter. Under conditions similar to those of the experiment in Ref. 1, the rate of scattered photons is very high, $\sim 10^5\ s^{-1}$, but most are rejected by the time-gating electronics. However, because the timing jitter of the SPAD detector is such that the prompt function exhibits a tail, a small but finite proportion ($\sim$0.02) will be passed by the time gate. To model the dependence on experimental parameters, note that the amount of scattered light from a volume element $dxdydz$ located at x, y, z within the probe region is expected to be linearly dependent on the relative laser intensity $I(x, y, z)$ and the relative light collection efficiency $C(x, y, z)$. Hence the net amount of scatter is expected to be linearly proportional to $\hat{C}\hat{I}V$, where

$$V = \iiint C(x, y, z)I(x, y, z)\mathrm{d}x\mathrm{d}y\mathrm{d}z \qquad (31)$$

is the volume of the probe region. In the simulation, Eq. (31) is evaluated with Monte Carlo integration and calls to the subroutines that evaluate C and I by Eqs. (28) and (7). Note, however, that the light scattering is not strictly isotropic, and the use of Eq. (28) within Eq. (31) yields only an approximate model for the dependence of light scatter on the experimental geometry. Nevertheless, within this approximation, because $\hat{I} \propto P/(\bar{\omega}_{y0}\bar{\omega}_{z0})$, the rate of promptly scattered light passed [or rejected] by the time gate is taken to be

$$b[b'] = \beta[\beta']VP\hat{C}/(\bar{\omega}_{y0}\bar{\omega}_{z0}), \qquad (32)$$

where the empirical constants are determined as

$$\beta[\beta'] = \bar{b}[\bar{b}']\bar{\omega}_{y0}\bar{\omega}_{z0}/(\bar{V}\bar{P}\bar{\hat{C}}), \qquad (33)$$

and in which quantities with an overbar have the values appropriate to the experimental conditions under which $\bar{b}[\bar{b}']$ were measured. The empirical constants $\beta[\beta']$ have the dimensions of counts per second per watt per meter. They account for the Raman cross section of a solvent molecule at the excitation wavelength, the overlap of the solvent Raman spectrum with the transmission of the spectral filters, the number of solvent molecules per unit volume, the number of photons per watt at the laser excitation wavelength, and the setting of the time gate. The functional dependence of the background count rate on experimental parameters given in Eq. (32) indicates that it is the thickness of the probe region along the direction of the laser propagation $V/(\bar{\omega}_{y0}\bar{\omega}_{z0})$ rather than the probe volume itself, which should be minimized to reduce the background.[10]

3. Induced Fluorescence of Solution Buffer Constituents and Optical Components

Certain solution buffer constituents may give rise to a low level of constant fluorescence background. Also, when scattered light strikes the microscope objective or spectral filter, these optics themselves fluoresce. Unlike unrejected scattered light, such induced fluorescence may possibly vary nonlinearly with $V, P, \hat{C}, \bar{\omega}_{y0}$, or $\bar{\omega}_{z0}$. Hence induced fluorescence can be difficult to model unless it has been first characterized accurately in a particular experiment. However, if stray fluorescence did occur and did vary linearly with the parameters, then its effects would be already be accounted for in the empirical constants $\beta[\beta']$.

4. SPAD Detector After-Pulses

Passively quenched SPAD detectors have dead times $\geq$200 ns and present negligible after-pulses. However, for actively quenched SPAD's with a dead time of $\sim$55 ns, after each photon detection event there is a probability $\epsilon \sim 2.1 \times 10^{-3}$ that charge trapping within the SPAD will lead to a second count, which will occur at a random time later and hence will usually be passed by the time-gating electronics.[21] After-pulses caused by fluorescence photons during the passage of molecules have little effect, but can be modeled by scaling the quantum efficiency of the SPAD by a factor of $1 + \epsilon$. However, after-pulses caused by promptly scattered photons that are themselves blocked by the time gate will cause the rate of background within the time gate to be increased. Under the experimental conditions of Ref. 1, the rate of promptly scattered photons is $\sim 3 \times 10^5\ s^{-1}$ and the rate of after-pulses $\sim$600 would be greater than the dark count rate $b_D \sim 50\ s^{-1}$. To determine the improvement anticipated from switching from a passively to actively quenched SPAD, such after-pulses can be modeled by scaling the empirical parameter β by a factor of $1 + \epsilon\beta'/\beta$. Note that if the parameter β were determined from experimental measurements already employing an actively quenched SPAD, then the value determined by Eq. (33) would already account for after-pulses.

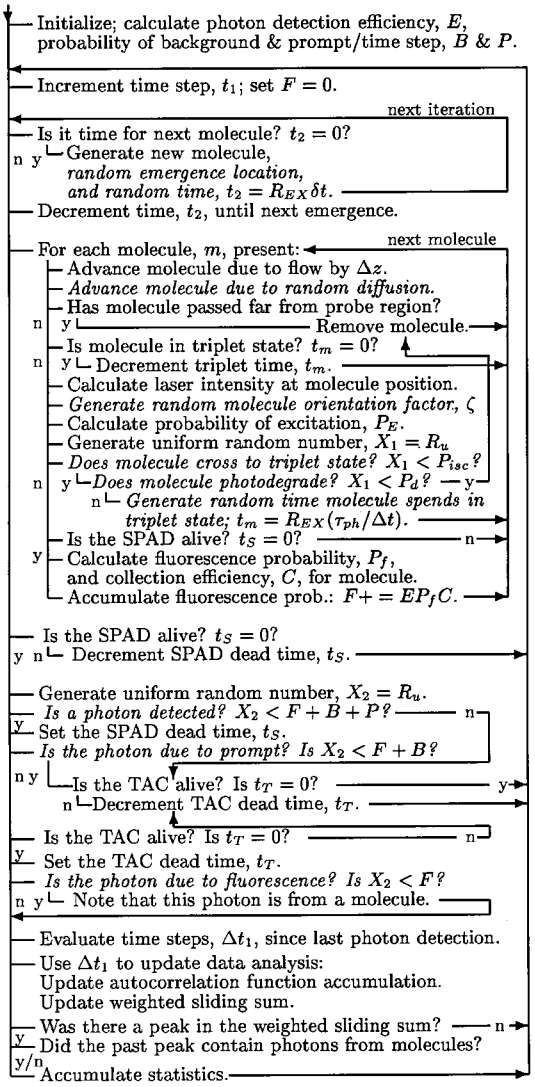

Fig. 3. Flow chart of overall simulation. All stochastic steps are indicated in italics.

E. Overall Simulation and Dead Times

Figure 3 displays a flow diagram of the overall simulation. Stochastic steps in the simulation are indicated in italics.

Upon initialization for the selected experimental parameters, the net fluorescence detection efficiency E, which accounts for the throughput of the optics, the spectral interference filter, and the time gate, and the quantum efficiency of the SPAD, is evaluated, together with the probability per iteration for detection of a background photon $B = (b + b_D)\Delta t$ or a promptly scattered photon $P = b'\Delta t$.

With each iteration, the simulation may introduce new molecules, and the advancement of all present molecules is due to the sheath flow and random diffusion. For each molecule that is not in the triplet manifold, the laser intensity at the molecules's position and the probability of excitation is evaluated and then used to stochastically determine if the molecule intersystem crosses or photodegrades during the current iteration. Then if the dead-time counter for the SPAD t_S is zero, indicating that the SPAD is currently responsive, the probability for detection of a fluorescence photon from the molecule P_f and the relative optical collection efficiency from the present location of the molecule C are evaluated. These are used to accumulate the net probability for detection of a fluorescence photon during the current iteration $F = E \sum P_f C\hat{C}$. A single uniform random number $X_2 = R_U$ is generated to determine whether a photon is detected, and if so, whether the photon passes through the time gate. If a photon is detected, t_S is set equal to the dead time of the SPAD divided by Δt, and it is decremented in subsequent iterations so as to count down the SPAD dead time, while still allowing the possibility for molecules to intersystem cross to the triplet manifold or to be photodestroyed. If the photon was passed by the time gate, the TAC will be activated; t_T is set equal to the dead time of the TAC divided by Δt and it is counted down in subsequent iterations, while still allowing the possibility for the SPAD to become paralyzed by a subsequent photon detection.

If a photon is detected within the time gate, X_2 is also used to determine whether the photon originated from a molecule or from background. This information would not be available in an experiment but is used by the simulation to acquire statistics on false and correct molecule detection events. Whenever a photon is detected within the time gate, the number of iterations since the last such detection, Δt_1, is evaluated and passed to a routine for updating the data analysis. The string of numbers generated by the simulation $\Delta t_1(p)$ is of the same form as the raw data accumulated experimentally in Ref. 1 with use of an analog-to-digital converter.

F. Data Processing

1. *Autocorrelation Function*

If a multichannel scalar were used to accumulate the photon count signal versus channel number, $s(n)$, then the digital autocorrelation function can be calculated as

$$G(m) = \sum_n s(n)s(n + m). \tag{34}$$

However, if the time represented by each channel is less than or equal to the TAC deadtime, then each channel will contain at most one photon, and the majority of channels will contain no photon. Only when $s(j) = 1$ and $s(k) = 1$ will $G(j + k)$ be incremented by 1. Hence if the form of the raw data instead consists of an array of delays between individual photons, $\Delta t_1(p)$, then the digital autocorrelation function is efficiently evaluated by accumulation of the prior delays; i.e., when the pth photon is detected with delay $\Delta t_1(p)$, the digital autocorrelation function $G(m)$ is incremented by 1 for $m = \Delta t_1(p)$, $\Delta t_1(p) + \Delta t_1(p - 1)$, $\Delta t_1(p) + \Delta t_1(p - 1) + \Delta t_1(p - 2)$, ... The two-line segment of the C code given

below illustrates the process, which is performed whenever a photon is detected within the time gate and can be implemented even more efficiently with pointers.

```
unsigned long int delta_t1[65536]=
 {G_LIMIT,0}, s,G[G_LIMIT]={0};
/*autocorrelation  function*/
unsigned short int p;/*wraps from 65535 to
  0*/
s=delta_t1[p=present_photon_number];
do{G[s]++;} while((s+=delta_t1[p--])
 <G_LIMIT);
```

The final shape of the autocorrelation function is expected to be approximately Gaussian for the following reason: If intersystem crossing and photodestruction do not occur, if diffusion is negligible, if the collection efficiency is uniform [$C(x, y, z) = 1$], and if the SPAD and TAC dead times are zero, then the mean fluorescence signal from a molecule transiting the Gaussian profile of the laser beam at a steady velocity would itself be a Gaussian of the form

$$\bar{s}(n) \propto \exp(-2n^2/\delta_t^2), \tag{35}$$

where

$$\delta_t = \bar{\omega}_{z0}/\Delta z \tag{36}$$

is the half-transit time. The autocorrelation function of relation (35) would then be a Gaussian with a standard deviation $\delta_t/\sqrt{2}$, and a curve fit could be used to find δ_t.

3. Weighted Sliding Sum

Improved distinction between photon bursts caused by molecules and random fluctuations in the background can be obtained by processing the signal $s(n)$ with a digital filter. For optimal filtering, the signal is convolved with a weighting function $w(k)$ that has the same profile as that of the pattern to be recognized. In the simulation, the weights are taken to be proportional to relation (35):

$$w(k) = \sqrt{2}\,\exp(-2k^2/\delta_t^2), \quad k = -q, \ldots, q, \tag{37}$$

where δ_t is known from Eq. (36) and q is the integer closest to δ_t. The filtered signal is

$$S(n) = \sum_{i=-q}^{k=q} s(n + k)w(k). \tag{38}$$

The prefactor of $\sqrt{2}$ is chosen for the weights in Eq. (37) so that when N photons occur in a burst with a profile proportional to relation (35), the peak value of the filtered signal is

$$\hat{S} = \sum_{k=-q}^{k=1} w(k)N(2/\sqrt{2\pi}\,\delta_t)\exp(-2k^2/\delta_t^2) \approx 0.95N. \tag{39}$$

Thus $\hat{S}$ is indicative of the number of detected photons within the burst, but it should be noted that if the burst has a different profile, $\hat{S}$ will also differ. For example, when two photons are detected at times $\pm q/2$, $\hat{S} \approx 0.6 \times 2$, but when they are detected close together in time, $\hat{S} \approx 1.4 \times 2$.

When the raw data consist of a sequence of delays $\Delta t(p)$, Eq. (38) can be evaluated efficiently as

$$S(n) = \sum_{-q<t_1(p)-n<q} w[t_1(p) - n], \tag{40}$$

where the photon arrival times $t_1(p)$ can be recalculated with $t_1(p) = t_1(p - 1) + \Delta t_1(p)$. Note that $S(n)$ varies gradually with n, and in the simulation it is evaluated in steps of $n = q/4$.

4. Results

A. Comparison with Past Experiment

Table 1 lists the values of parameters used to simulate the experiment of Ref. 1.

Figure 4(a) illustrates the geometry of the experiment. The focused laser beam is shown as an open elliptical cylinder, the region for which the relative collection efficiency $C(x, y, z)$ is 1 is shown as a wire-grid double conic and its projection, the 1-μm-diameter opening of the injection capillary is shown as a small circle at the base of the figure, and the trajectories of three molecules are shown emerging from the circle and passing through the laser beam. The times during which the molecules have intersystem crossed to the triplet manifold are indicated by the darker segments. The seventh and ninth molecules photodegrade as they transit the beam, but the ninth molecule still generates a detectable photon burst.

The individual photons detected during the passage of the sixth molecule are shown in Fig. 4(b), together with the output from a weighted sliding sum (wss) digital filter in which the same weighting function as that in Ref. 1 is used to process the data. The wss output over a longer duration is shown in Fig. 4(c) together with the histogram of peak amplitudes obtained after the passage of 10,000 molecules over a simulated period of 54 s. The histogram exhibits a distinct valley at an amplitude of ~13. The presence of this valley indicates that most molecules pass through the central part of the probe region and do so without photodegradation, thereby yielding photon bursts that are clearly distinguishable from background fluctuations. Note that if a simple flow cell were used, or if the injection capillary opening were large, or the sheath flow velocity small, the molecule trajectories would not form a narrow stream, and many molecules would pass outside of, or near the edges of, the probe region and so yield small amplitude photon bursts. In this case, the histogram of peak amplitudes would be clearly monotonic. The histogram of peak amplitudes is found to agree reasonably well with that experimentally obtained (Fig. 11 of Ref. 1), although the valley is not quite so deep in the experimental results, probably because of a 5–10% fluctuation in the laser power that was not accounted for in the simulation.

Table 1. Parameters Used to Simulate Experiment of Ref. 1

Symbol	Description	Value
	Laser parameters	
λ	Wavelength	0.585 μm
E_γ	Photon energy	3.4×10^{-19} J
R	Repetition rate	7.6×10^{7} s^{-1}
$\bar{\omega}_{y0}$	Beam waist in y dimension	4.8 μm
$\bar{\omega}_{z0}$	Beam waist in z dimension	9.6 μm
M_i^2	For nonideal Gaussian beam	1.3
$\bar{P}$	Average power	0.014 W
	Molecule parameters[9]	
σ_a	Absorption cross section	3.7×10^{-16} cm^2
Φ_f	Fluorescence quantum efficiency	0.35
Φ_{isc}	Intersystem crossing efficiency	0.002
Φ_d	Photodestruction efficiency	5.5×10^{-5}
τ_f	Fluorescence lifetime	4.6 ns
τ_{ph}	Phosphorescence lifetime	4.0 μs
D	Translational diffusion coefficient	450 μm^2 s^{-1}
	Geometry and flow	
r_p	Spatial filter pinhole radius	400 μm
M	Collection objective magnification	60
NA	Objective numerical aperture	0.85
r_0	Injection capillary tip radius	0.5 μm
z_0	Injection capillary location	-15 μm
δ_t	Half-transit time	0.5 ms
δt_m	Mean time between molecules	5.3×10^{-3} s
	Detector parameters	
E	Throughput of optics and time Gate $\times$ SPAD quantum efficiency	0.1
S_D	SPAD dead time	800 ns
T_D	TAC dead time	2.5 μs
	Background parameters	
b_D	SPAD dark count rate	50 s^{-1}
$\bar{b}$	Scattered photons passed	3×10^{5} s^{-1}
$\bar{b}'$	Scattered photons rejected by time gate	5880 s^{-1}
V	Calculated probe volume	1.9×10^{-15} m^3
β	Coefficient for scatter passed	0.09 (ps Wm)$^{-1}$
β'	Coefficient rejected by time gate	4.6 (ps Wm)$^{-1}$

[a]Ref. 27.

Molecules can be counted by counting wss peaks of amplitude greater than the value at the valley. Under the conditions of the experiment in Ref. 1 as listed in Table 1, there are 7653 such peaks, although 65 of these are due to fluctuations in the background noise. Overall, the molecule detection efficiency is 76%, which is slightly lower than the 80% value estimated in the experimental research. The detection efficiency is lowered at high counting rates because two or more molecules sometimes pass simultaneously and generate only one photon burst. The number of molecules that become photodestroyed is 2577, although 1607 of these generate individually detectable photon bursts. In Ref. 1 it was estimated that ~20% of molecules escape detection because of photodegradation, but the results of the simulation indicate that the value is <10%.

Figure 4(d) shows the autocorrelation function of the simulated data together with a Gaussian curve fit, from which a half-transit time of $\delta_t = 0.513$ ms is obtained, which is in close agreement with the set value of 0.5 ms. In the experimental research, an additional exponential-shaped peak superposed on the Gaussian was observed (Fig. 6 of Ref. 1). This was originally thought to be due to fluctuations in the fluorescence signal because of intersystem crossing or photodegradation, but the simulation indicates that it is more likely to be due to laser power or flow rate fluctuations.

B. Feasibility of More Rapid Single-Molecule Detection

Versions of the simulation that employ real-time graphics and menu-adjustable experimental parameters have allowed quick exploration of the performance of the experiment throughout the parameter space. When the laser power, flow rate, experimental geometry, and dead times are varied, it becomes evident that the electronic dead times of the SPAD and TAC, together with the high rate of promptly scattered background photons, limit the ability to obtain detectable photon bursts when shorter molecular transit times are used. However, actively quenched SPAD's with shorter dead times[21] and time-gated photon detection without the use of a TAC[28] have recently been developed. Also, the rate of promptly scattered background can be decreased by reducing the size of the laser beam waists and spatial filter pinhole, but the flow rate must be increased suitably to avoid diffusional loss and other parameters adjusted to maintain an adequate signal-to-noise ratio for SMD. When such changes are made, the simulation indicates that experiments for more rapid detection should be possible, even with the relatively poor quantum yield offered by the particular dye molecule used in this research. Table 2 lists the parameters with values that are altered from those in Table 1, and Fig. 5 displays the histogram of peak amplitudes obtained after passage of 10,000 molecules over 54 s. In total, 8126 molecules generate wss bursts of amplitude ≥ 8, and there are 125 false detection events. The number of molecules that become photodestoyed is 1475, although 1380 of these generate detectable photon bursts. An experiment following the design parameters of Table 2 has recently been conducted, yielding results that agree well with the simulation predictions and demonstrate an order-of-magnitude decrease in the time required for detection of each molecule.[29]

Intersystem crossing to the triplet manifold becomes increasingly more important for faster detection conditions. Figure 6 shows that the autocorrelation function obtained under the conditions of Table 2 exhibits an additional peak near the origin, with a decay constant equal to the phosphorescence lifetime τ_{ph}. When τ_{ph} is altered in the simulation, the decay constant of the peak also changes, and when ϕ_{isc} is altered, the relative magnitude of the peak changes. This indicates that the kinetics associated with intersystem crossing should be measurable by SMD experiments.[30]

5. Discussion and Conclusions

The Monte Carlo simulation described above is useful for gaining confidence in the interpretation of exper-

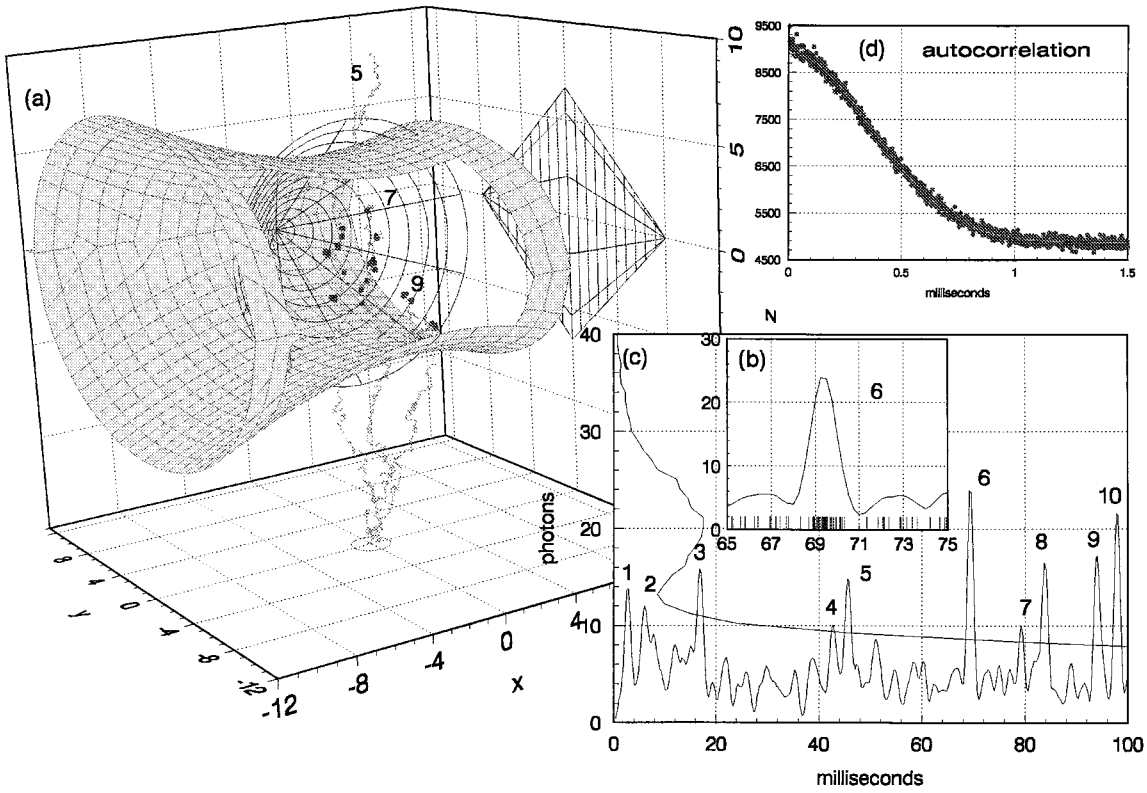

Fig. 4. Results of simulation under conditions of Table 1. (a) Geometry of probe region, showing focused laser beam, region of maximum collection efficiency (wire grid), and trajectories of three molecules, with darker segments indicating that the molecule is in the triplet manifold; (b) individual photons and output from weighted sliding sum (wss) during transit of molecule 6; (c) output from wss during passage of ten molecules, with histogram of peak amplitudes from 10,000 molecules drawn against the y ordinate; (d) autocorrelation function and Gaussian curve fit.

imental results, for improving one's quantitative understanding of the trade-offs and limitations that photophysical and instrumental parameters play in the choice of experimental setup, and for optimizing the choice of parameters for a particular SMD application. The simulation yields results that agree quantitatively with past experimental results, and it has proved to be an invaluable tool for choosing parameters in the design of improved experiments. An order-of-magnitude decrease in the transit time required for efficient detection has recently been achieved by following the predictions of the simulation.[29] The simulation indicates that other modifications will enable future experiments to achieve detection with transit times as short as ~10 μs and with moderate efficiencies, limited mainly by the quantum efficiency for intersystem crossing.

The effects of the adjustable parameters, detector and electronic hardware, optical design, and molecule parameters on the outcome of a SMD experiment are

Table 2. Changes in Parameters for Rapid Detection

Symbol	Description	Value
$\bar{\omega}_{y0}$	Beam waist in y dimension	3.5 μm
$\bar{\omega}_{z0}$	Beam waist in z dimension	3.5 μm
$\bar{P}$	Average power	0.04 W
r_p	Spatial filter pinhole radius	250 μm
δ_t	Half-transit time	0.05 ms
S_D	SPAD dead time	65 ns
T_D	TAC dead time	0 μs
β	Coefficient for scatter passed	0.10 (ps Wm)$^{-1}$
β′	Coefficient rejected by time gate	4.6 (ps Wm)$^{-1}$
V	Calculated probe volume	1.3×10^{-15} m^3
$\bar{b}$	Scattered photons passed	4.9×10^4 s^{-1}
$\bar{b}'$	Scattered photons rejected by time gate	2.2×10^6 s^{-1}

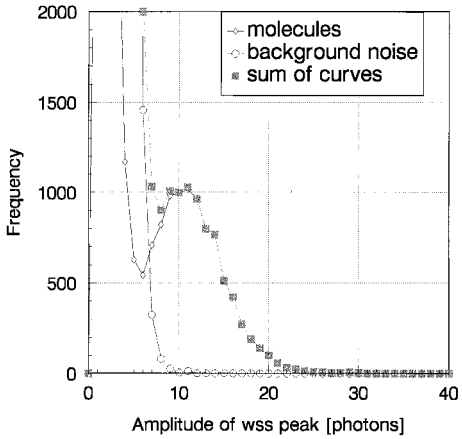

Fig. 5. Histogram of peak amplitudes under fast detection conditions.

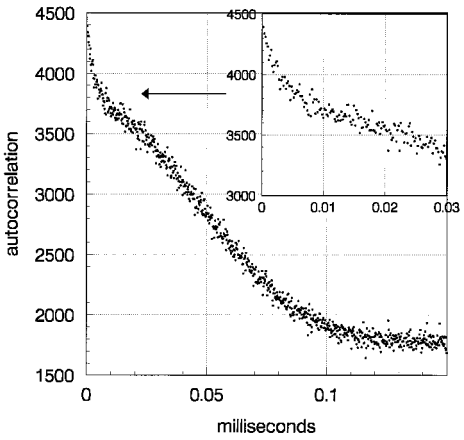

Fig. 6. Autocorrelation function under fast detection conditions.

nonlinearly interrelated and complicated. The Monte Carlo simulation can help determine whether significant changes in optical design and hardware warrant an investment of experimental resources. The ability to more accurately design experiments and predict their outcomes increases the importance for accurate knowledge of the photophysical parameters of the various dyes and solvent conditions that may be used for different applications. In most cases, these parameters are not available in the literature, but can be measured by standard procedures.[27] Even without accurate knowledge of such parameters, one can gain useful information by estimating the range that the parameters fall within and by considering the predicted outcome of an experiment as the parameters are varied within that range.

The simulation can be adapted readily to investigate various features of ultrasensitive detection experiments. Other applications that it has been used for include (1) investigation of alternate signal processing schemes; (2) learning of procedures for precise optical alignment of experiments by use of real-time graphical feedback of simulated count rates and processed data (photon-burst histograms, autocorrelation functions, etc.), while alignment parameters such as x_i in Eq. (8) are varied; (3) investigation of methods for spectroscopic measurements on individually detected molecules and for distinguishing different types of molecules[20]; and (4) investigation of use of fluorescence correlation spectroscopy for resolution of multiple diffusion coefficients from the autocorrelation function.

This research was supported in part by the National Science Foundation grant CTS-9512489. We thank C. Parigger for assistance with the Silicon Graphics Indigo 2 and Power Challenge L workstations and K. Kimble for introducing us to VOGL graphics.

References and Notes

1. L. Q. Li and L. M. Davis, "Rapid and efficient detection of single chromophore molecules in aqueous solution," Appl. Opt. **34,** 3208–3217 (1995); and references cited therein.
2. E. B. Shera, N. K. Seitzinger, L. M. Davis, R. A. Keller, and S. A. Soper, "Detection of single fluorescent molecules," Chem. Phys. Lett. **174,** 553–557 (1990).
3. K. Kneipp, Y. Wang, H. Kneipp, L. T. Perelman, I. Itzkan, R. R. Dasari, and M. S. Feld, "Single molecule detection using surface-enhanced Raman scattering (SERS)," Phys. Rev. Lett. **78,** 1667–1670 (1997).
4. S. Nie and S. R. Emory, "Probing single nanoparticles by surface enhanced Raman scattering," Science **275,** 1102–1106 (1997).
5. L. Q. Li and L. M. Davis, "Single photon avalanche diode for single molecule detection," Rev. Sci. Instrum. **64,** 1524–1529 (1993).
6. S. A. Soper, Q. L. Mattingly, and P. Vegunta, "Photon burst detection of single near-infrared fluorescent molecules," Anal. Chem. **65,** 740–747 (1993).
7. Y. H. Lee, R. G. Maus, B. W. Smith, and J. D. Winefordner, "Laser-induced fluorescence detection of a single molecule in a capillary," Anal. Chem. **66,** 4142–4149 (1994).
8. M. Eigen and R. Rigler, "Sorting single molecules: application to diagnostics and evolutionary biotechnology," Proc. Natl. Acad. Sci. USA **91,** 5740–5747 (1994).
9. S. Nie, D. T. Chiu, and R. N. Zare, "Probing individual molecules with confocal fluorescence microscopy," Science **266,** 1018–1021 (1994).
10. X. H. Xu and E. S. Yeung, "Direct measurement of single-molecule diffusion and photodecomposition in free solution," Science **275,** 1106–1109 (1997).
11. J. Mertz, C. Xu, and W. W. Webb, "Single-molecule detection by two-photon-excited fluorescence," Opt. Lett. **20,** 2532–2534 (1995).
12. P. M. Goodwin, R. L. Affleck, W. P. Ambrose, J. H. Jett, M. E. Johnson, J. C. Martin, J. T. Petty, J. A. Schecker, M. Wu, and R. A. Keller, "Detection of single fluorescent molecules in flowing sample streams," in *Computer Assisted Analytical Spectroscopy*, S. D. Brown, ed. (Wiley, Sussex, England, 1996), pp. 61–80.
13. S. Nie, D. T. Chiu, and R. N. Zare, "Real-time detection of single molecules in solution by confocal fluorescence microscopy," Anal. Chem. **67,** 2849–2857 (1995).
14. L. M. Davis and L. Q. Li, "Monte Carlo model of a single molecule counting experiment," in *Laser Applications to Chemical Analysis*, Vol. 5 of 1994 OSA Technical Digest Series (Optical Society of America, Washington, D.C., 1994), pp. 206–209.
15. R. A. Mathies, K. Peck, and L. Stryer, "Optimization of high-sensitivity fluorescence detection," Anal. Chem. **62,** 1786–1791 (1990).
16. L. M. Davis, L. Q. Li, E. B. Shera, A. Castro, and S. A. Soper, "Photon statistics for the detection of single molecules in solution," in *Quantum Electronics and Laser Science*, Vol. 13 of OSA Technical Digest Series (Optical Society of America (Washington, D.C., 1992), pp. 70–72.
17. S. A. Soper, L. M. Davis, and E. B. Shera, "Detection and identification of single molecules in solution," J. Opt. Soc. Am. B **9,** 1761–1769 (1992).
18. C. Zander, M. Sauer, K. H. Drexage, D. S. Ko, A. Schultz, J. Wolfrum, L. Brand, C. Eggeling, and C. A. M. Seidel, "Detection and characterization of single molecules in aqueous solution," Appl. Phys. B **63,** 517–523 (1996).
19. D. H. Bunfield, "Simulation of a single molecule detection experiment," M.S. thesis (University of Tennessee, Knoxville, Tennessee, 1997).
20. L. M. Davis and D. H. Bunfield, "Spectroscopic identification of individually detected fluorescent molecules," *The Fifth International Conference on Methods and Applications of Fluorescence Spectroscopy, Berlin, 1997. Book of Abstracts*, W. Rettig, ed. (Springer-Verlag, Berlin, 1997), p. 27.

21. A. Spinelli, L. M. Davis, and H. Dautet, "Actively quenched single-photon avalanche diode for high repetition rate time-gated photon counting," Rev. Sci. Instrum. **67,** 55–61 (1996).
22. J. C. Fister III, S. C. Jacobson, L. M. Davis, and J. M. Ramsey, "Counting single-chromophore molecules for ultrasensitive analysis and separations on microchip devices," Anal. Chem. **70,** 431–437 (1997).
23. One significant application currently under development that demands efficient and unambiguous SMD is rapid DNA sequencing. Also, efficient processing of the sample is desirable for assay of miniscule sample quantities, such as the components of a single cell and genetic screening without DNA amplification by polymerase chain reaction. See references of Ref. 1.
24. R. Loudon, *The Quantum Theory of Light*, 2nd ed. (Oxford University, New York, 1973), pp. 78–81.
25. A. Penzkofer, W. Falkenstein, and W. Kaiser, "Vibronic relaxation in the S_1 state of rhodamine dye solutions," Chem. Phys. Lett. **44,** 82–87 (1976).
26. H. Qian and E. L. Elson, "Analysis of confocal laser-induced microscope optics for 3-D fluorescence correlation spectroscopy," Appl. Opt. **30,** 1185–1195 (1991).
27. S. A. Soper, H. L. Nutter, R. A. Keller, L. M. Davis, and E. B. Shera, "The photophysical constants of several fluorescent dyes pertaining to ultrasensitive fluorescence spectroscopy," Photochem. Photobiol. **57,** 972–977 (1993).
28. L. M. Davis, L. E. Schneider, and D. B. Bunfield, "Increasing the rate of detection of single molecules in solution," in *Laser Applications to Chemical, Biological, and Environmental Analysis, Vol. 3 of 1996 OSA Technical Digest Series* (Optical Society of America, Washington, D.C., 1996), pp. 24–26.
29. L. M. Davis, "Efficient counting of single molecules with sub-100 μs transit times," paper BC.06 at American Physical Society SES97 meeting, Nashville, November 1997, http://aps.org/BAPSSES97/abs/S700006.html/.
30. J. Widengren, R. Rigler, and U. Mets, "Triplet-state monitoring by fluorescence correlation spectroscopy," J. Fluorescence **4,** 255–258 (1994).